

# Measurement of the branching fraction for the decay $K_S \rightarrow \pi\mu\nu$ with the KLOE detector

The KLOE-2 Collaboration

D. Babusci<sup>d</sup>, M. Berlowski<sup>v</sup>, C. Bloise<sup>d</sup>, F. Bossi<sup>d</sup>, P. Branchini<sup>s</sup>,  
 A. Budano<sup>r,s</sup>, B. Cao<sup>u</sup>, F. Ceradini<sup>r,s</sup>, P. Ciambrone<sup>d</sup>, F. Curciarello<sup>a,d</sup>,  
 E. Czerwiński<sup>c</sup>, G. D'Agostini<sup>n,o</sup>, E. Danè<sup>d</sup>, V. De Leo<sup>n,o</sup>, E. De Lucia<sup>d</sup>,  
 A. De Santis<sup>d</sup>, P. De Simone<sup>d</sup>, A. Di Cicco<sup>r,s</sup>, A. Di Domenico<sup>n,o</sup>,  
 D. Domenici<sup>d</sup>, A. D'Uffizi<sup>d</sup>, A. Fantini<sup>p,q</sup>, P. Fermani<sup>d</sup>, S. Fiore<sup>t,o</sup>, A. Gajos<sup>c</sup>,  
 P. Gauzzi<sup>n,o</sup>, S. Giovannella<sup>d</sup>, E. Graziani<sup>s</sup>, V. L. Ivanov<sup>g,h</sup>, T. Johansson<sup>u</sup>,  
 X. Kang<sup>d</sup>, D. Kisielewska-Kamińska<sup>c</sup>, E. A. Kozyrev<sup>g,h</sup>, W. Krzemien<sup>v</sup>,  
 A. Kupsc<sup>u</sup>, P. A. Lukin<sup>g,h</sup>, G. Mandaglio<sup>f,b</sup>, M. Martini<sup>d,m</sup>, R. Messi<sup>p,q</sup>,  
 S. Miscetti<sup>d</sup>, D. Moricciani<sup>d</sup>, P. Moskal<sup>c</sup>, S. Parzych<sup>c</sup>, A. Passeri<sup>s</sup>, V. Patera<sup>l,o</sup>,  
 E. Perez del Rio<sup>n,o</sup>, P. Santangelo<sup>d</sup>, M. Schioppa<sup>j,k</sup>, A. Selce<sup>r,s,\*</sup>, M. Silarski<sup>c</sup>,  
 F. Sirghi<sup>d,e</sup>, E. P. Solodov<sup>g,h</sup>, L. Tortora<sup>s</sup>, G. Venanzoni<sup>i</sup>, W. Wiślicki<sup>v</sup>,  
 M. Wolke<sup>u</sup>

<sup>a</sup>*Dipartimento di Fisica e Astronomia "Ettore Majorana", Università di Catania, Italy*

<sup>b</sup>*INFN Sezione di Catania, Catania, Italy.*

<sup>c</sup>*Institute of Physics, Jagiellonian University, Cracow, Poland.*

<sup>d</sup>*Laboratori Nazionali di Frascati dell'INFN, Frascati, Italy.*

<sup>e</sup>*Horia Hulubei National Institute of Physics and Nuclear Engineering, Măgurele, Romania*

<sup>f</sup>*Dipartimento di Scienze Matematiche e Informatiche, Scienze Fisiche e Scienze della Terra dell'Università di Messina, Messina, Italy.*

<sup>g</sup>*Budker Institute of Nuclear Physics, Novosibirsk, Russia.*

<sup>h</sup>*Novosibirsk State University, Novosibirsk, Russia.*

<sup>i</sup>*INFN Sezione di Pisa, Pisa, Italy.*

<sup>j</sup>*Dipartimento di Fisica dell'Università della Calabria, Rende, Italy.*

<sup>k</sup>*INFN Gruppo collegato di Cosenza, Rende, Italy.*

<sup>l</sup>*Dipartimento di Scienze di Base ed Applicate per l'Ingegneria dell'Università "Sapienza", Roma, Italy.*

<sup>m</sup>*Dipartimento di Scienze e Tecnologie applicate, Università "Guglielmo Marconi", Roma, Italy.*

<sup>n</sup>*Dipartimento di Fisica dell'Università "Sapienza", Roma, Italy.*

<sup>o</sup>*INFN Sezione di Roma, Roma, Italy.*

<sup>p</sup>*Dipartimento di Fisica dell'Università "Tor Vergata", Roma, Italy.*

<sup>q</sup>*INFN Sezione di Roma Tor Vergata, Roma, Italy.*

<sup>r</sup>*Dipartimento di Matematica e Fisica dell'Università "Roma Tre", Roma, Italy.*

<sup>s</sup>*INFN Sezione di Roma Tre, Roma, Italy.*

<sup>t</sup>*ENEA, Department of Fusion and Technology for Nuclear Safety and Security, Frascati (RM), Italy*

<sup>u</sup>*Department of Physics and Astronomy, Uppsala University, Uppsala, Sweden.*

<sup>v</sup>*National Centre for Nuclear Research, Warsaw, Poland.*

---

\*Corresponding author

Email address: [andrea.selce@roma3.infn.it](mailto:andrea.selce@roma3.infn.it) (A. Selce)

---

**Abstract**

Based on a sample of 300 million  $K_S$  mesons produced in  $\phi \rightarrow K_L K_S$  decays recorded by the KLOE experiment at the DAΦNE  $e^+e^-$  collider we have measured the branching fraction for the decay  $K_S \rightarrow \pi\mu\nu$ . The  $K_S$  mesons are identified by the interaction of  $K_L$  mesons in the detector. The  $K_S \rightarrow \pi\mu\nu$  decays are selected by a boosted decision tree built with kinematic variables and by a time-of-flight measurement. Signal efficiencies are evaluated with data control samples of  $K_L \rightarrow \pi\mu\nu$  decays. A fit to the reconstructed muon mass distribution finds  $7223 \pm 180$  signal events. Normalising to the  $K_S \rightarrow \pi^+\pi^-$  decay events the result for the branching fraction is  $\mathcal{B}(K_S \rightarrow \pi\mu\nu) = (4.56 \pm 0.11_{\text{stat}} \pm 0.17_{\text{syst}}) \times 10^{-4}$ .

*Keywords:*  $e^+e^-$  collisions,  $K^0$  meson, semileptonic decay

---

**1. Introduction**

The branching fraction for semileptonic decays of charged and neutral kaons together with the lifetime measurements are used to determine the  $|V_{us}|$  element of the Cabibbo–Kobayashi–Maskawa quark mixing matrix. The relation among the matrix elements of the first row,  $|V_{ud}|^2 + |V_{us}|^2 + |V_{ub}|^2 = 1$ , provides the most stringent test of the unitarity of the quark mixing matrix. Different factors contribute to the uncertainty in determining  $|V_{us}|$  from kaon decays [1, 2, 3] and among the six semileptonic decays the contribution of the lifetime uncertainty is smallest for the  $K_S$  meson. Nevertheless, given the lack of pure high-intensity  $K_S$  meson beams compared with  $K^\pm$  and  $K_L$  mesons, the  $K_S \rightarrow \pi e\nu$  decay provides the least precise determination of  $|V_{us}|$ , and the branching fraction  $\mathcal{B}(K_S \rightarrow \pi\mu\nu)$  has not yet been measured.

We present a measurement of the  $K_S \rightarrow \pi\mu\nu$  branching fraction performed by the KLOE experiment at the DAΦNE  $\phi$ -factory of the Frascati National Laboratory based on an integrated luminosity of  $1.6 \text{ fb}^{-1}$ . DAΦNE [4] is an electron–positron collider running at the centre-of-mass energy of 1.02 GeV colliding  $e^+$  and  $e^-$  beams at an angle of  $\pi - 0.025$  rad and with a bunch-crossing period of 2.71 ns. The  $\phi$  mesons are produced with a small transverse momentum of 13 MeV and  $K_L$ – $K_S$  pairs are produced almost back-to-back with a cross section  $\times$  branching fraction of about  $1 \mu\text{b}$ . The beam energy, the energy spread, the beams transverse momentum and the position of the interaction point are measured with high accuracy with Bhabha scattering events [5].

The  $K_S$  ( $K_L$ ) mesons are identified (*tagged*) with high efficiency and purity by the observation of a  $K_L$  ( $K_S$ ) meson in the opposite hemisphere. This tagging procedure allows the selection efficiency for  $K_S \rightarrow \pi\mu\nu$  to be evaluated with good accuracy using a sample of the abundant decay  $K_L \rightarrow \pi\mu\nu$  tagged by the detection of  $K_S \rightarrow \pi^+\pi^-$  decays. The branching fraction is extracted

normalising the number of  $K_S \rightarrow \pi\mu\nu$  events to the number of  $K_S \rightarrow \pi^+\pi^-$  events recorded in the same dataset.

## 2. The KLOE detector

The detector consists of a large-volume cylindrical drift chamber, surrounded by a lead-scintillating fibers finely-segmented calorimeter. A superconducting coil around the calorimeter provides a 0.52 T axial magnetic field. The beam pipe at the interaction region is spherical in shape with 10 cm radius, made of a 0.5 mm thick beryllium-aluminum alloy. Low-beta quadrupoles are located at  $\pm 50$  cm from the interaction region. Two small lead-scintillating-tile calorimeters [6] are wrapped around the quadrupoles.

The drift chamber [7], 4 m in diameter and 3.3 m long, has 12582 drift cells arranged in 58 concentric rings with alternated stereo angles and is filled with a low-density gas mixture of 90% helium–10% isobutane. The chamber shell is made of carbon fiber-epoxy composite with an internal wall of 1.1 mm thickness at 25 cm radius. The spatial resolution is  $\sigma_{xy} = 0.15$  mm and  $\sigma_z = 2$  mm in the transverse and longitudinal projection, respectively. The momentum resolution for long tracks is  $\sigma_{p_T}/p_T = 0.4\%$ . Tracks vertices are reconstructed with a spatial resolution of about 3 mm.

The calorimeter [8] is divided into a barrel and two endcaps and covers 98% of the solid angle. The readout granularity is  $4.4 \times 4.4$  cm<sup>2</sup>, for a total of 2440 cells arranged in five layers. Each cell is read out at both ends by photomultipliers. The energy deposits are obtained from signal amplitudes and the arrival time and the position along the fibers are obtained from time differences. Cells close in time and space are grouped into energy clusters. The cluster energy  $E$  is the sum of the cell energies, the cluster time and position are energy-weighted averages. Energy and time resolutions are  $\sigma_E/E = 0.057/\sqrt{E}$  (GeV) and  $\sigma_t = 54$  ps/ $\sqrt{E}$  (GeV)  $\oplus$  100 ps, respectively. The cluster spatial resolution is  $\sigma_{\parallel} = 1.4$  cm/ $\sqrt{E}$  (GeV) along the fibers and  $\sigma_{\perp} = 1.3$  cm in the orthogonal direction.

The level-1 trigger [9] uses both the calorimeter and the drift chamber information; the calorimeter trigger requires two energy deposits with  $E > 50$  MeV in the barrel and  $E > 150$  MeV in the endcaps; the drift chamber trigger is based on the number and topology of hit drift cells. A higher-level cosmic-ray veto rejects events with at least two energy deposits above 30 MeV in the outermost calorimeter layer. The trigger time is determined by the first particle reaching the calorimeter and is synchronised with the DAΦNE r.f. signal. The time interval between bunch crossings is smaller than the time spread of the signals produced by the particles, thus the event  $T_0$  related to the bunch crossing originating the event is determined after event reconstruction and all the times related to that event are shifted accordingly. Data for reconstruction are selected by an on-line filter [10] to reject beam backgrounds. The filter also streams the events into different output files for analysis according to their properties and topology (event classification). A fraction of 5% of the events

are recorded without applying the filter to control the efficiency of the event classification.

### 3. Data sample and event preselection

Processes of interest for the analysis are simulated with the **GEANFI** [10] program for an integrated luminosity equal to that of the data. Calorimeter energy deposits and drift chamber hits from beam background events triggered at random are overlaid onto the simulated events. The simulated events are processed with the same reconstruction algorithms as the data.

Kaons from  $\phi$ -meson decays are emitted in two opposite hemispheres with mean decay path  $\lambda_S = 5.9$  mm and  $\lambda_L = 3.4$  m, thus about 50% of  $K_L$  mesons reach the calorimeter before decaying. The velocity of the  $K_L$  in the  $\phi$  reference system is  $\beta^* = 0.22$ .  $K_S$  mesons are tagged by  $K_L$  interactions in the calorimeter,  $K_L$ -crash in the following, with a clear signature of a delayed cluster not associated to tracks. The following requirements are applied to select  $K_L$ -crash:

- a cluster with energy  $E_{\text{clu}} > 100$  MeV not associated to tracks (neutral cluster); the centroid of the neutral cluster defines the  $K_L$  direction with a resolution of  $\sim 1^\circ$ ;
- polar angle of the neutral cluster  $15^\circ < \theta_{\text{clu}} < 165^\circ$  to suppress small-angle beam backgrounds;
- $0.17 < \beta^* < 0.28$  for the velocity in the  $\phi$  reference system of the particle originating the neutral cluster;  $\beta^*$  is obtained from the velocity in the laboratory system,  $\beta = r_{\text{clu}}/ct_{\text{clu}}$ , with  $t_{\text{clu}}$  being the cluster time and  $r_{\text{clu}}$  the distance from the nominal interaction point, the  $\phi$  momentum and the angle between the  $\phi$  momentum and the  $K_L$ -crash direction.

These requirements are used to tag  $K_S$  mesons. Assigning the neutral kaon mass, the  $K_S$  4-momentum is defined by the  $K_L$ -crash direction and the  $\phi$  4-momentum:  $P_{K_S} = P_\phi - P_{K_L}$ .

The  $K_S \rightarrow \pi\mu\nu$  candidates are selected requiring two tracks of opposite curvature forming a vertex inside the cylinder defined by

$$\rho_{\text{vtx}} = \sqrt{x_{\text{vtx}}^2 + y_{\text{vtx}}^2} < 5 \text{ cm} \quad |z_{\text{vtx}}| < 10 \text{ cm}. \quad (1)$$

The above requirements represent the preselection.

After preselection, the data sample contains about 300 million events and its composition, as evaluated by Monte Carlo simulation (MC), is shown in Table 1. The large majority of events are  $K_S \rightarrow \pi^+\pi^-$  decays, and there is also a large contribution from  $\phi \rightarrow K^+K^-$  events where one kaon or its decay products generate a fake  $K_L$ -crash and the other kaon decays early into  $\pi^\pm\pi^0$ .

The distribution of  $\beta^*$  is shown in Figure 1 for data and simulated events. Two peaks are visible, the first is associated to events triggered by photons or electrons, and the second to events triggered by charged pions. The trigger is

Table 1: Number of data and simulated events after preselection.

	Events [ $10^3$ ]	Fraction [%]
Data	301646	
MC	312019	
$K_S \rightarrow \pi^+ \pi^-$	301976	96.78
$\phi \rightarrow K^+ K^-$	9566	3.07
$K_S \rightarrow \pi e \nu$	259	0.08
$K_S \rightarrow \pi \mu \nu$	140	0.04
$K_S \rightarrow \pi^0 \pi^0$	30	0.01
Others	47	0.02

synchronised with the bunch crossing and the time difference between a photon (or electron) and a pion (or muon) arriving at the calorimeter corresponds to about one bunch-crossing shift.

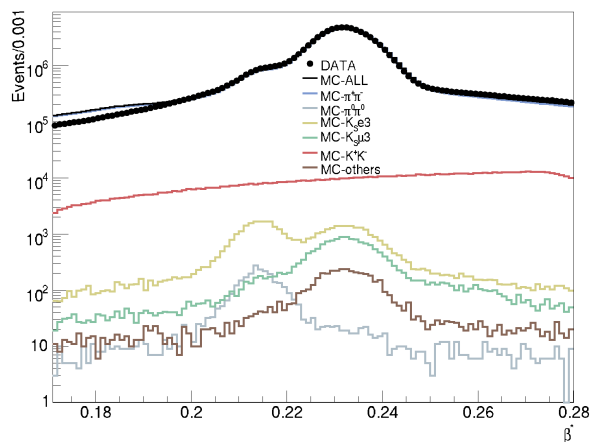


Figure 1: Distribution of  $\beta^*$  after preselection for data and simulated events.

#### 4. Selection of signal and normalisation events

The selection of signal events is performed in two steps; first a selection based on the event kinematics using only tracking variables, second a selection based on the time-of-flight measured with the calorimeter. The two groups of variables are uncorrelated. To assign a time to the tracks connected to the vertex each track is associated to an energy cluster. The track-to-cluster association (TCA) is applied as follows: for each track connected to the vertex a cluster with  $E_{\text{clu}} > 20$  MeV and  $15^\circ < \theta_{\text{clu}} < 165^\circ$  is required whose centroid is within

60 cm of the track extrapolation to the calorimeter wall. Only if TCA is satisfied by both tracks the event is retained.

Five variables with good discriminating power against background are used in a multivariate analysis. A boosted decision tree (BDT) classifier is built with the following variables:

- $\vec{p}_1, \vec{p}_2$  : the tracks momenta;
- $\alpha_{1,2}$  : the angle at the vertex between the two momenta in the  $K_S$  reference system;
- $\alpha_{SL}$  : the angle between the momentum sum,  $\vec{p}_{\text{sum}} = \vec{p}_1 + \vec{p}_2$ , and the  $K_L$ -crash direction;
- $\Delta p$  : the difference between  $|\vec{p}_{\text{sum}}|$  and the  $K_S$  momentum determined using the tagging  $K_L$ ;
- $m_{\pi\pi}$  : the invariant mass reconstructed from  $\vec{p}_1$  and  $\vec{p}_2$ , in the hypothesis of charged-pion mass.

The distributions of the variables are shown in Figure 2 for data and simulated events.

Two additional cuts are applied to suppress the background in the tails of the distributions:

$$p < 320 \text{ MeV for both tracks} \quad \text{and} \quad \Delta p < 190 \text{ MeV.} \quad (2)$$

The training of the BDT classifier is done on a simulated sample of 5,000  $K_S \rightarrow \pi\mu\nu$  events and a sample of 50,000 background events; samples of the same size are used for the test. After training and test the classification is run on all events of the MC and data sample. The distribution of the BDT classifier output is shown in Figure 3 for data and simulated events. The data distribution is well reproduced by simulation in the region populated by the signal. To suppress the large background of  $K_S \rightarrow \pi^+\pi^-$  and  $\phi \rightarrow K^+K^-$  events, a cut is applied

$$BDT > 0.18 \quad (3)$$

chosen to maximise the ratio  $S/\sqrt{S+B}$  where  $S$  and  $B$  are the signal and background yields.

The track pairs in the selected events are  $\pi\pi$ ,  $K\pi$ ,  $e\pi$  for the main backgrounds and  $\mu\pi$  for the signal, a selection based on time-of-flight measurement is performed to identify  $\mu\pi$  pairs. For each track associated to a cluster, the difference between the time-of-flight measured by the calorimeter and the time-of-flight measured along the particle trajectory

$$\delta t_i = t_{\text{clu},i} - L_i/c\beta_i \quad i = 1, 2$$

is computed, where  $t_{\text{clu},i}$  is the time associated to track  $i$ ,  $L_i$  is the length of the track, and the velocity  $\beta_i = p_i/\sqrt{p_i^2 + m_i^2}$  is function of the mass hypothesis

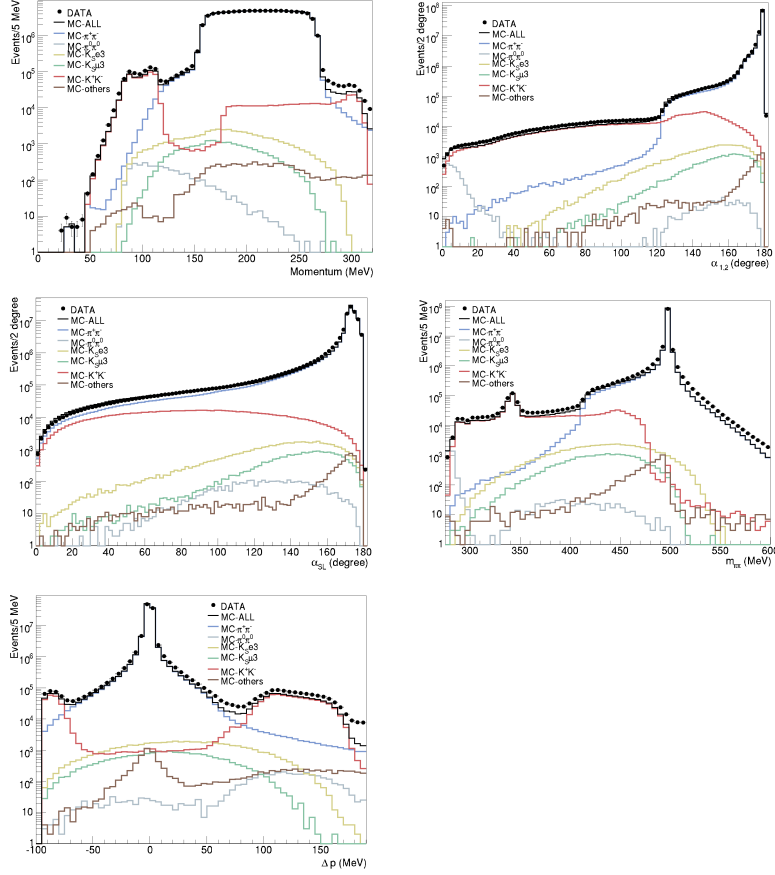


Figure 2: Distributions of the variables used in the multivariate analysis for data and simulated events after preselection. From top left: track momenta  $(p_1, p_2)$ , angle between the two tracks in the  $K_S$  reference system  $(\alpha_{1,2})$ , angle between  $K_L$  and  $K_S$  directions  $(\alpha_{SL})$ , two-track invariant mass in the hypothesis of charged pions  $(m_{\pi\pi})$ ,  $\Delta p = |\vec{p}_{\text{sum}} + \vec{p}_{K_L}|$ .

for track  $i$ . The times  $t_{\text{clu},i}$  are referred to the trigger and the same  $T_0$  value is assigned to both clusters. To reduce the uncertainty from the determination of  $T_0$  the difference

$$\delta t_{1,2} = \delta t_1 - \delta t_2$$

is used to determine the mass assignment to the tracks. The  $\pi\pi$  hypothesis is tested first, the distribution of  $\delta t_{\pi\pi} = \delta t_{1,\pi} - \delta t_{2,\pi}$  is shown in Figure 4(left). A fair agreement is observed between data and simulation, the  $K_S \rightarrow \pi\mu\nu$  and  $K_S \rightarrow \pi e\nu$  distributions are well separated and the  $K^+K^-$  background is isolated in the tails of the distribution, however the signal is hidden under a large  $K_S \rightarrow \pi^+\pi^-$  background. To reduce the background a cut is applied

$$1 \text{ ns} < |\delta t_{\pi\pi}| < 3 \text{ ns}. \quad (4)$$

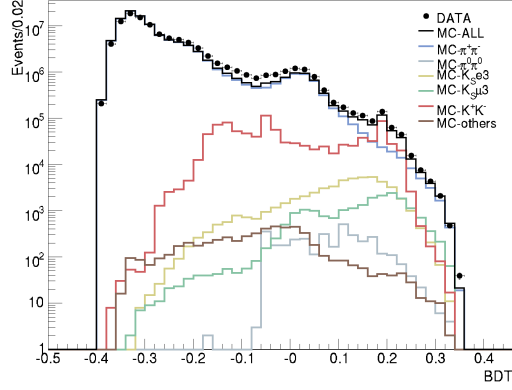


Figure 3: Distribution of the BDT classifier output for data and simulated events.

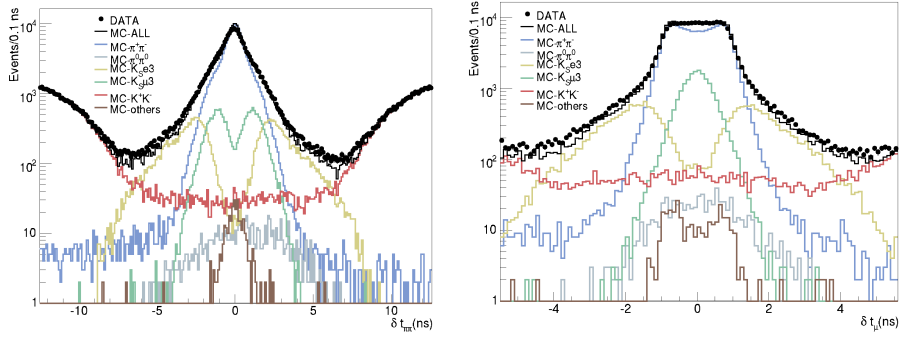


Figure 4: Distributions of  $\delta\pi\pi$  (left) and  $\delta t_\mu = \min[|\delta t_{\pi\mu}|, |\delta t_{\mu\pi}|]$  (right) for data and simulated events.

The  $\pi\mu$  hypothesis is tested by assigning the pion and muon mass to either track

$$\delta t_{\pi\mu} = \delta t_{1,\pi} - \delta t_{2,\mu} \quad \text{and} \quad \delta t_{\mu\pi} = \delta t_{1,\mu} - \delta t_{2,\pi}.$$

The two-dimensional  $\delta t_{\pi\mu} \times \delta t_{\mu\pi}$  distribution for simulated signal events indicates that the correct mass assignment corresponds to the smaller absolute value of the two hypotheses. The distribution of the signed value of  $\delta t_\mu = \min[|\delta t_{\pi\mu}|, |\delta t_{\mu\pi}|]$  is shown in Figure 4(right) for data and simulated events. The distribution for the signal is narrow and peaked at zero while it is broader for the backgrounds. A final cut is applied

$$|\delta t_\mu| < 0.5 \text{ ns.} \quad (5)$$

The number of selected events in the data sample is 38686 and its composition as evaluated by simulation is listed in Table 2. After the mass assignment



Table 2: Number of events after the  $\delta t_\mu$  selection for data and simulated events.

	Events	Fraction [ % ]
Data	38686	
MC	36444	
$K_S \rightarrow \pi^+\pi^-$	25853	70.9
$\phi \rightarrow K^+K^-$	475	1.30
$K_S \rightarrow \pi e\nu$	448	1.23
$K_S \rightarrow \pi\mu\nu$	9424	25.9
Others	244	0.7

to the two tracks the invariant mass of the charged particle identified as the muon is evaluated as

$$m_\mu^2 = (E_{K_S} - E_\pi - p_{\text{miss}})^2 - p_\mu^2$$

with  $p_{\text{miss}}^2 = (\vec{p}_{K_S} - \vec{p}_\pi - \vec{p}_\mu)^2$ ,  $E_{K_S}$  and  $\vec{p}_{K_S}$  being the energy and momentum reconstructed using the tagging  $K_L$ , and  $\vec{p}_\pi$ ,  $\vec{p}_\mu$ , the momenta of the pion and muon track.

The number of signal events is extracted with a fit to the  $m_\mu^2$  distribution with the MC shapes of three components:  $K_S \rightarrow \pi\mu\nu$ ,  $K_S \rightarrow \pi^+\pi^-$  and the sum of all other backgrounds. The fit is performed in the range  $-6000 < m_\mu^2 < 24000$  MeV<sup>2</sup> with 48 degrees of freedom. The third component, which is peaked around  $m_e^2$ , is constrained to a negligible value by the fit. Figure 5 shows the distribution of  $m_\mu^2$  for data, simulated events and the fit, and Table 3 presents the result of the fit. The number of signal events is

$$N_{\pi\mu\nu} = 7223 \pm 180 \quad \text{with } \chi^2/\text{ndf} = 30/48.$$

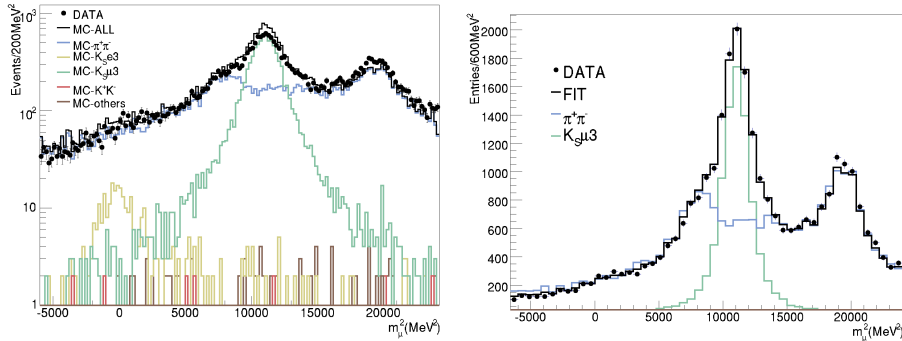


Figure 5: The  $m_\mu^2$  distribution for data, MC signal and background (left); comparison of data with the fit (right).

Table 3: Result of the fit to the  $m_\mu^2$  distribution.

	Fraction	Events
$\pi\mu\nu$	0.23	$7223 \pm 180$
$\pi^+\pi^-$	0.77	$23764 \pm 270$
Total		30987

The normalisation sample of  $K_S \rightarrow \pi^+\pi^-$  events is selected by requiring  $140 < p < 280$  MeV for both tracks (Figure 2). This requirement selects  $N_{\pi\pi} = (282.314 \pm 0.017) \times 10^6$  events with a purity of 99.9% as determined by simulation.

## 5. Determination of efficiencies

The branching fraction for the  $K_S \rightarrow \pi\mu\nu$  decay is evaluated as

$$\mathcal{B}(K_S \rightarrow \pi\mu\nu) = \frac{N_{\pi\mu\nu}}{\epsilon_{\pi\mu\nu}} \times \frac{\epsilon_{\pi\pi}}{N_{\pi\pi}} \times R_\epsilon \times \mathcal{B}(K_S \rightarrow \pi^+\pi^-), \quad (6)$$

where  $N_{\pi\mu\nu}$  and  $N_{\pi\pi}$  are the numbers of  $K_S \rightarrow \pi\mu\nu$  and  $K_S \rightarrow \pi^+\pi^-$  events,  $\epsilon_{\pi\mu\nu}$  and  $\epsilon_{\pi\pi}$  are the respective selection efficiencies, and  $R_\epsilon = (\epsilon_{\pi\pi}/\epsilon_{\pi\mu\nu})_{\text{com}}$  is the ratio of common efficiencies for the trigger, on-line filter and preselection that can be different for the two decays.

The efficiencies for the selection of the signal sample (SS) are determined with two different  $K_L \rightarrow \pi\mu\nu$  control samples (CS) and evaluated as

$$\epsilon_{\text{SS}}^{\text{data}} = \epsilon_{\text{CS}}^{\text{data}} \times \frac{\epsilon_{\text{SS}}^{\text{MC}}}{\epsilon_{\text{CS}}^{\text{MC}}}, \quad (7)$$

where  $\epsilon_{\text{CS}}^{\text{data}}$  is the efficiency of the control sample, corrected for the MC purities before and after a given selection, and  $\epsilon_{\text{SS}}^{\text{MC}}$ ,  $\epsilon_{\text{CS}}^{\text{MC}}$  are the efficiencies obtained from simulation for the signal and control samples, respectively.

The  $K_L \rightarrow \pi\mu\nu$  decay [11, 12] is kinematically identical to the signal, the only difference being the much longer decay path. For the control sample the tagging is done with  $K_S \rightarrow \pi^+\pi^-$  decays, preselected in the same way as for the signal sample with the additional cut  $|m_{\pi\pi} - m_{K^0}| < 15$  MeV to increase the purity. The radial distance of the second vertex, the  $K_L$  vertex, is required to be smaller than 5 cm to match the signal selection, but greater than 1 cm to minimise the ambiguity in identifying the  $K_L$  and  $K_S$  vertices. The control sample is composed mainly of  $K_L \rightarrow \pi e \nu$  ( $\mathcal{B} = 0.405$ ),  $K_L \rightarrow \pi^+\pi^-\pi^0$  ( $\mathcal{B} = 0.125$ ) and  $K_L \rightarrow \pi\mu\nu$  ( $\mathcal{B} = 0.270$ ) decays, while most of  $K_L \rightarrow \pi^0\pi^0\pi^0$  decays are rejected requiring the vertex. The distribution of the missing mass,  $m_{\text{miss}}^2$ , respect to the two tracks connected to the  $K_L$  vertex, assigning the charged-pion mass, shows a narrow isolated peak at the  $\pi^0$  mass; a cut  $m_{\text{miss}}^2 < 15000$  MeV<sup>2</sup> efficiently

rejects the  $K_L \rightarrow \pi^+\pi^-\pi^0$  decays. The number of events in the control sample is 911757.

The analysis presented in Section 4 is divided in two steps: selection based on kinematic variables and selection based on time-of-flight (TOF) and the two groups of variables are largely uncorrelated. The selections of the two control samples are made as follows:

- a cut on the TOF variables is applied to evaluate the efficiency of the selection based on the kinematic variables and the BDT classifier;
- a cut on kinematic variables is applied to evaluate the efficiency of the TCA and TOF selections.

The control sample for evaluating the efficiencies of the selection with kinematic variables and BDT classifier is selected applying a cut on the two-dimensional  $\delta t_{\pi\mu} \times \delta t_{\mu\pi}$  distribution that removes most of the  $K_L \rightarrow \pi e \nu$  events. The purity of the sample as determined with simulation is 86%. The resolutions in the measurement of the tagging  $K_S$  (control sample) are similar to those of the tagging  $K_L$  (signal sample) and the same BDT classifier is used for both samples. The BDT MC distributions for the signal and control sample are compared in Figure 6(left). Applying to the control sample the same selections as for the signal, Eqs. (2) and (3), the efficiencies evaluated with Eq. (7) are

$$\epsilon(\text{kinem. sel.}) = 0.982 \pm 0.004_{\text{stat}} \quad \text{and} \quad \epsilon(\text{BDT}) = 0.417 \pm 0.003_{\text{stat}}.$$

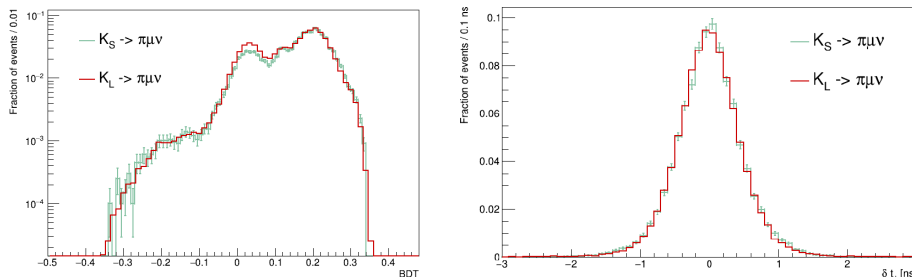


Figure 6: Normalised Monte Carlo distributions of the BDT classifier output (left) and  $\delta t_{\mu}$  (right) for  $K_L \rightarrow \pi\mu\nu$  and  $K_S \rightarrow \pi\mu\nu$  events.

The control sample for evaluating the TCA and TOF efficiencies is selected applying a cut on the  $m_{\pi\pi} \times m_{\text{miss}}^2$  distribution, where  $m_{\text{miss}}$  is the mass recoiling against the  $\pi^+\pi^-$  system, to reject  $K_L \rightarrow \pi e \nu$  events. In the  $K_S \rightarrow \pi\mu\nu$  analysis the  $T_0$  is determined by the first cluster in time, associated with one of the daughter particles of the  $K_S$  decay; then for the control sample it is required that the first cluster in time be associated with the  $K_L$  decay in order not to bias the TOF variables. The purity of the sample as determined with simulation is 87%. The MC distributions of  $\delta t_{\mu}$  for the signal and control sample

are compared in Figure 6(right). Applying to the control sample the analysis procedure as for the signal the efficiencies evaluated with Eq. (7) are

$$\epsilon(\text{TCA}) = 0.347 \pm 0.002_{\text{stat}} \quad \text{and} \quad \epsilon(\text{TOF}) = 0.392 \pm 0.003_{\text{stat}}.$$

The tails of the  $m_\mu^2$  distribution in Figure 5(left) are not included in the fit to improve its stability, the relative efficiency is  $0.991 \pm 0.001$ . Combining the values accounting for correlations we obtain  $\epsilon_{\pi\mu\nu} = 0.0552 \pm 0.0005$ . The signal selection efficiencies are summarised in Table 4 where only the statistical errors are shown.

Table 4: Efficiencies for the signal selections. The errors are statistical, the error of the total efficiency accounts for correlations of the single errors.

Selection	Efficiency
Kinematic selection	$0.982 \pm 0.004$
BDT selection	$0.417 \pm 0.003$
TCA selection	$0.347 \pm 0.002$
TOF selection	$0.392 \pm 0.003$
FIT range	$0.991 \pm 0.001$
Total	$0.0552 \pm 0.0005$

The ratio  $R_\epsilon$  in Eq. (6) results from several effects all depending on the global properties of the event: trigger, on-line filter, event classification,  $T_0$  determination,  $K_L$ -crash and  $K_S$  identification. The various contributions to  $R_\epsilon$  evaluated with simulation are listed in Table 5 where only the statistical errors are shown.

Table 5: Contributions to the ratio of efficiencies  $R_\epsilon$  in Eq. (6). The error on  $R_\epsilon$  is calculated as the quadratic sum of the errors of the single ratios.

Selection	$R_\epsilon = (\epsilon_{\pi\pi}/\epsilon_{\pi\mu\nu})_{\text{com}}$
Trigger	$1.0649 \pm 0.0005$
On-line filter	$1.0113 \pm 0.0002$
Event classification	$1.1406 \pm 0.0007$
$T_0$ determination	$1.0135 \pm 0.0002$
$K_L$ -crash and $\beta^*$	$1.1283 \pm 0.0022$
$K_S$ identification	$1.0481 \pm 0.0012$
$R_\epsilon$	$1.472 \pm 0.004$

The efficiency of the  $K_S \rightarrow \pi^+\pi^-$  normalisation sample for the momentum selection  $140 < p < 280$  MeV is measured using the preselected data by varying the cut on the vertex transverse position, as in Eq. (1), in 1 cm steps from  $\rho_{\text{vtx}}^{\text{max}} = 1$  cm to  $\rho_{\text{vtx}}^{\text{max}} = 4$  cm, based on the observation that  $\rho_{\text{vtx}}$  and the tracks

momenta are very loosely correlated. Using Eq. (7) to correct for the purities before and after the momentum cut and extrapolating to  $\rho_{\text{vtx}}^{\text{max}} = 5$  cm the efficiency is  $\epsilon_{\pi\pi}^{\text{data}} = (96.569 \pm 0.004)\%$ . Alternatively, the efficiency is evaluated using the  $K_S \rightarrow \pi^+\pi^-$  data sample (with  $\rho_{\text{vtx}}^{\text{max}} = 5$  cm and  $\epsilon_{\pi\pi}^{\text{MC}} = \epsilon_{\text{pres}}^{\text{MC}}$ ) correcting for the purity for the cut in momentum:  $\epsilon_{\pi\pi}^{\text{data}} = (96.657 \pm 0.002)\%$ . The difference between the two values is taken as systematic uncertainty. The number of  $K_S \rightarrow \pi^+\pi^-$  events corrected for the efficiency is

$$N_{\pi\pi}/\epsilon_{\pi\pi} = (292.08 \pm 0.27) \times 10^6.$$

## 6. Systematic uncertainties

Three main systematic uncertainties affect the signal count: BDT and time-of-flight selection, and the  $m_\mu^2$  fit.

The distributions of the BDT classifier output for the data and simulated signal and control sample events are in good agreement as shown in Figures 3 and 6. The resolution of the BDT variable predicted by simulation comparing the reconstructed events with those at generation level is  $\sigma_{\text{BDT}} = 0.005$ . The analysis is repeated varying the BDT cut of Eq. (3), the number of signal events is found to be stable and the rms value of the differences gives a relative uncertainty of 0.3%.

The main source of uncertainty in the TOF selection is the cut on  $\delta t_{\pi\pi}$  in Eq. (4) because the signal and background distributions in Figure 4(left) are steep and with opposite slopes; the subsequent selection on  $\delta t_\mu$  in Eq. (5) has a minor effect. The resolution of the  $\delta t_{\pi\pi}$  variable evaluated with simulation and  $K_S \rightarrow \pi^+\pi^-$  data control samples is  $\pm 0.27$  ns. The analysis is repeated varying the  $\delta t_{\pi\pi}$  lower cut in the range 0.5–1.25 ns, the rms value of the differences gives a relative uncertainty of  $\pm 3.0\%$ . This is the main systematic uncertainty affecting the measurement.

The fit to the  $m_\mu^2$  distribution in Figure 5 is repeated varying the range and the bin size, the relative systematic uncertainty is 0.3%.

The dependence of  $R_\epsilon$  on systematic effects has been studied in previous analyses for different  $K_S$  decays selected with the  $K_L$ -crash method:  $K_S \rightarrow \pi^+\pi^-$  and  $K_S \rightarrow \pi^0\pi^0$  [13], and  $K_S \rightarrow \pi e \nu$  [14]. The systematic uncertainties are evaluated by a comparison of data with simulation.

**Trigger** – Two triggers are used for recording the events, the calorimeter trigger and the drift chamber trigger. The validation of the MC relative efficiency is derived from the comparison of the single-trigger and coincidence rates with the data. The data over MC ratio is 0.999 with negligible error.

**On-line filter and event classification** – The event classification produces different streams for the analyses. The  $K_L K_S$  stream selects events based on the properties of  $K_S$  and  $K_L$  decays. In more than 99% of the cases the events are selected based on the  $K_S$  decay topology and the  $K_L$ -crash signature and differences between MC and data are accounted for in the systematic uncertainties derived below for the  $K_S$  identification and  $K_L$ -crash.

**T<sub>0</sub>** – The trigger time is synchronised with the r.f. signal and the event T<sub>0</sub> is re-defined after event reconstruction. The systematic uncertainty is evaluated analysing the data and MC distributions of T<sub>0</sub> for the decays with the most different timing properties:  $K_S \rightarrow \pi^+\pi^-$  and  $K_S \rightarrow \pi^0\pi^0$  [13]. The data over MC ratios show that the uncertainty of the relative efficiency is less than 0.1%.

**K<sub>L</sub>-crash and β\* selection** – The systematic uncertainty is evaluated comparing data and simulated events tagged by  $K_S \rightarrow \pi^+\pi^-$  and  $K_S \rightarrow \pi^0\pi^0$  decays which have different timing and topology characteristics. The data over MC ratio is 1.001 with negligible error.

**K<sub>S</sub> identification** – The systematic uncertainty due to the requirement of two tracks forming a vertex in the cylinder defined by Eq. (1) is evaluated separately for signal and normalisation samples. The first is evaluated with  $K_L \rightarrow \pi\mu\nu$  events selected with the same vertex requirements as for the signal but tagged by  $K_S \rightarrow \pi^0\pi^0$  decays. For the  $K_S \rightarrow \pi^+\pi^-$  sample the efficiency is evaluated by tagging with  $K_L$ -crash and removing the requirement of the vertex. Combining the two values gives a data over MC ratio of  $1.002 \pm 0.017$  where the error is due to the purity of the samples.

The  $R_\epsilon$  total systematic uncertainty is estimated by combining the differences from one of the data over MC ratios and amounts to 1.7%.

Including the systematic uncertainties the factors in Eq. (6) are:

$$\epsilon_{\pi\mu\nu} = 0.0552 \pm 0.0017 \quad \text{and} \quad R_\epsilon = 1.472 \pm 0.025.$$

All systematic uncertainties are summarised in Table 6.

Table 6: Summary of systematic uncertainties of  $\epsilon_{\pi\pi}$ ,  $\epsilon_{\pi\mu\nu}$  and  $R_\epsilon$ .

Source	$\epsilon_{\pi\pi}$ [ % ]	$\epsilon_{\pi\mu\nu}$ [ % ]	$R_\epsilon$ [ % ]
$K_S \rightarrow \pi^+\pi^-$ selection	0.1		
BDT selection		0.3	
TOF selection		3.0	
Fit $m_\mu^2$ distribution		0.3	
MC and CS statistics		0.8	
Trigger			0.1
T <sub>0</sub> determination			<0.1
$K_L$ -crash and β*			0.1
$K_S$ identification			1.7
Total	0.1	3.1	1.7

## 7. Result

From Eq. (6) with  $N_{\pi\mu\nu} = 7223 \pm 180$ ,  $N_{\pi\pi}/\epsilon_{\pi\pi} = (292.08 \pm 0.27) \times 10^6$ , the values of the efficiencies  $\epsilon_{\pi\mu\nu} = 0.0552 \pm 0.0017$ ,  $R_\epsilon = 1.472 \pm 0.025$ , and the

value  $\mathcal{B}(K_S \rightarrow \pi^+\pi^-) = 0.69196 \pm 0.00051$  measured by KLOE [14], we derive the branching fraction

$$\mathcal{B}(K_S \rightarrow \pi\mu\nu) = (4.56 \pm 0.11_{\text{stat}} \pm 0.17_{\text{syst}}) \times 10^{-4} = (4.56 \pm 0.20) \times 10^{-4}.$$

This is the first measurement of this decay mode. In comparison, assuming universality of the kaon-lepton coupling, the expected value [15] is

$$\mathcal{B}(K_S \rightarrow \pi\mu\nu) = \mathcal{B}(K_S \rightarrow \pi e\nu) \times R(I_K^\ell) \times \frac{1 + \delta_{\text{LD}}^{\pi\mu\nu}}{1 + \delta_{\text{LD}}^{\pi e\nu}} = (4.69 \pm 0.06) \times 10^{-4}$$

as derived from the value of the branching fraction  $\mathcal{B}(K_S \rightarrow \pi e\nu)$  measured by KLOE [13], the ratio  $R(I_K^\ell)$  of the phase space integrals for the semileptonic decays  $K_L \rightarrow \pi\mu\nu$  and  $K_L \rightarrow \pi e\nu$  measured by KTeV [16], and the contributions of long-distance radiative corrections to the semileptonic kaon decays [17].

## 8. Conclusion

A measurement of the branching fraction for the decay  $K_S \rightarrow \pi\mu\nu$  is presented based on data collected with the KLOE experiment at the DAΦNE  $e^+e^-$  collider corresponding to an integrated luminosity of  $1.6 \text{ fb}^{-1}$ . The  $\phi \rightarrow K_L K_S$  decays are exploited to select samples of pure and quasi-monochromatic  $K_S$  mesons and data control samples of  $K_L \rightarrow \pi\mu\nu$  decays. The  $K_S \rightarrow \pi\mu\nu$  decays are selected by a boosted decision tree built with kinematic variables and by a measurement of time-of-flight. The efficiencies for detecting the  $K_S \rightarrow \pi\mu\nu$  decays are derived from  $K_L \rightarrow \pi\mu\nu$  data control samples. A fit to the  $m_\mu^2$  distribution finds  $7223 \pm 180$  signal events. Normalising to  $K_S \rightarrow \pi^+\pi^-$  decay events, the result for the branching fraction is  $\mathcal{B}(K_S \rightarrow \pi\mu\nu) = (4.56 \pm 0.11_{\text{stat}} \pm 0.17_{\text{syst}}) \times 10^{-4}$  to be compared with the expected value of  $(4.69 \pm 0.06) \times 10^{-4}$ .

**Acknowledgements** – We warmly thank our former KLOE colleagues for the access to the data collected during the KLOE data taking campaign. We thank the DAΦNE team for their efforts in maintaining low background running conditions and their collaboration during all data taking. We thank our technical staff: G.F. Fortugno and F. Sborzacchi for their dedication in ensuring efficient operation of the KLOE computing facilities; M. Anelli for his continuous attention to the gas system and detector safety; A. Balla, M. Gatta, G. Corradi and G. Papalino for electronics maintenance; C. Piscitelli for his help during major maintenance periods. This work was supported in part by the Polish National Science Centre through the Grants No. 2013/11/B/ST2/04245, 2014/14/E/ST2/00262, 2014/12/S/ST2/00459, 2016/21/N/ST2/01727, 2016/23/N/ST2/01293, 2017/26/M/ST2/00697.

## References

- [1] M. Antonelli et al., An evaluation of  $|V_{us}|$  and precise tests of the Standard Model from world data on leptonic and semileptonic kaon decays, *Eur. Phys. J. C* **69** (2010) 399, arXiv:1005.2323 [hep-ph].

- [2] M. Moulson, Experimental determination of  $V_{us}$  from kaon decays, 9th International Workshop on the CKM Unitarity Triangle, 28 November - 3 December 2016, Tata Institute for Fundamental Research, Mumbai, India, arXiv:1704.04104 [hep-ex]
- [3] F. Ambrosino et al.,  $|V_{us}|$  and lepton universality from kaon decays with the KLOE detector, JHEP **04** (2008) 059, arXiv:hep-ex/0802.3009.
- [4] A. Gallo et al., DAΦNE Status Report, European Particle Accelerator Conference, 26-30 June 2006, Edinburgh, Scotland, Conf. Proc. C060626 (2006) 604.
- [5] F. Ambrosino et al., Measurement of the DAΦNE luminosity with the KLOE detector using large angle Bhabha scattering, Eur. Phys. J. C **47** (2006) 589, arXiv:hep-ex/0604048.
- [6] M. Adinolfi et al., The QCAL tile calorimeter of KLOE, Nucl. Instrum. Meth. A **483** (2002) 649.
- [7] M. Adinolfi et al., The tracking detector of the KLOE experiment, Nucl. Instrum. Meth. A **488** (2002) 51.
- [8] M. Adinolfi et al., The KLOE electromagnetic calorimeter, Nucl. Instrum. Meth. A **482** (2002) 364.
- [9] M. Adinolfi et al., The trigger system of the KLOE experiment, Nucl. Instrum. Meth. A **492** (2002) 134.
- [10] F. Ambrosino et al., Data handling, reconstruction and simulation for the KLOE experiment, Nucl. Instrum. Meth. A **534** (2004) 403, arXiv:physics/0404100.
- [11] F. Ambrosino et al., Measurements of the absolute branching ratios for the dominant  $K_L$  decays, the  $K_L$  lifetime and  $V_{us}$  with the KLOE detector, Phys. Lett. B **632** (2006) 43, arXiv:hep-ex/0509045.
- [12] F. Ambrosino et al., Measurement of the  $K_L \rightarrow \pi\mu\nu$  form factor parameters with the KLOE detector, JHEP **12** (2007) 105, arXiv:0710.4470 [hep-ex].
- [13] F. Ambrosino et al., Precise measurement of  $\Gamma(K_S \rightarrow \pi^+\pi^-(\gamma))/\Gamma(K_S \rightarrow \pi^0\pi^0)$ , with the KLOE detector at DAΦNE, Eur. Phys. J. C **48** (2006) 767, arXiv:hep-ex/0601025.
- [14] F. Ambrosino et al., Study of the branching ratio and charge asymmetry for the decay  $K_S \rightarrow \pi e\nu$  with the KLOE detector, Phys. Lett. B **636** (2006) 173, arXiv:hep-ex/0601026.
- [15] M. Tanabashi et al. (Particle Data Group), The Review of Particle Physics, Phys. Rev. D **98** (2018) 030001.
- [16] T. Alexopoulos et al., Measurements of semileptonic  $K_L$  decay form factors, Phys. Rev. D **70** (2004) 092007, arXiv:hep-ex/0406003.
- [17] C. T. André, Radiative corrections in  $K_{e3}^0$  decays, Annals Phys. **332** (2007) 2518, arXiv:hep-ph/0406006.